Angewandte
International Edition Chemie

DOI: 10.1002/anie.201407053

Carbon-Rich Porphyrins

Superbenzene–Porphyrin Conjugates**

Dominik Lungerich, Jakob F. Hitzenberger, Mario Marcia, Frank Hampel, Thomas Drewello, and Norbert Jux**

Abstract: *A free-base porphyrin carrying two hexabenzocoronene (HBC) substituents in a trans arrangement and its zinc complex have been prepared. The compounds were characterized extensively and found to form tricationic dimers in the gas phase. X-ray crystallography confirms for the zinc complex a profound π-stacking of the HBC moieties. In contrast, the free-base porphyrin incarcerates n-heptane which essentially prevents π-stacking. Upon excitation of the HBC substituents, efficient energy transfer to the central porphyrin is observed.*

In recent years, efforts have been made to extend the substituents on porphyrins from common phenyl and aryl groups to larger polycyclic aromatic hydrocarbons (PAHs) including naphthyl, pyrenyl, and even coronenyl groups.[1] Typically substitution is associated with a bathochromic shift of the absorption of these compounds compared to the absorption of the parent tetraphenylporphyrin (TPP). The properties can be further influenced upon fusion of porphyrin and substituents through the formation of an additional bond between the substituent and the β-pyrrolic position of the porphyrin core.[2] However, in these systems, the porphyrin moiety is still the dominating part determining the properties of the molecular superstructure. Only little is known about carbon-rich porphyrins with structural features that are dominated by large PAHs. While in TPP the phenyl moieties mainly impart solubility, large PAHs are predestined to have a profound impact on the molecular properties paving the way towards novel materials for nanoelectronics. Due to its size and electronic properties, hexa-*peri*-hexabenzocoronene (HBC)—"superbenzene"[3]—comes to mind as the almost ideal candidate to investigate this matter.[4] Nonetheless, only little is known about superbenzene–porphyrin conjugates, since their synthesis faces considerable difficulties.[5]

Herein we present a straightforward synthetic strategy towards those carbon-rich conjugates taking advantage of soluble superbenzene derivatives. The impressively high solubility of fivefold *tert*-butylated HBC aldehyde **1**[6] in common organic solvents, such as dichloromethane, makes this molecule a versatile building block for the construction of larger carbon-rich architectures and is key to a successful porphyrin synthesis. Compound **1** was successfully condensed with functionalized dipyrromethane **2**[7]—chosen because it provides further handles for functionalization—to obtain the HBC–porphyrin conjugate **3** in high yield (Scheme 1). The reaction was carried out under mild Lindsey conditions,[8] with application of catalytic $BF_3 \cdot OEt_2$ as a Lewis acid, followed by oxidation with 2,3-dichloro-5,6-dicyano-1,4-benzoquinone (DDQ). Conjugate **3** was obtained as a dark red solid after chromatography. Subsequent metalation of **3** by reaction with $Zn(OAc)_2 \cdot 2\,H_2O$ in THF under reflux gave the Zn^{II} derivative **4** in quantitative yield. The first structural evidence for the desired conjugate **3** came from the ^1H NMR spectrum: a pronounced downfield shift towards $\delta = 10.18$ ppm for the four HBC protons adjacent to the porphyrin core, a broad multiplet at around $\delta = 9.37$ ppm for the remaining twenty HBC protons, doublets at $\delta = 9.15$ and 8.83 ppm for the β-pyrrylic protons, and the inner-NH protons of the porphyrin

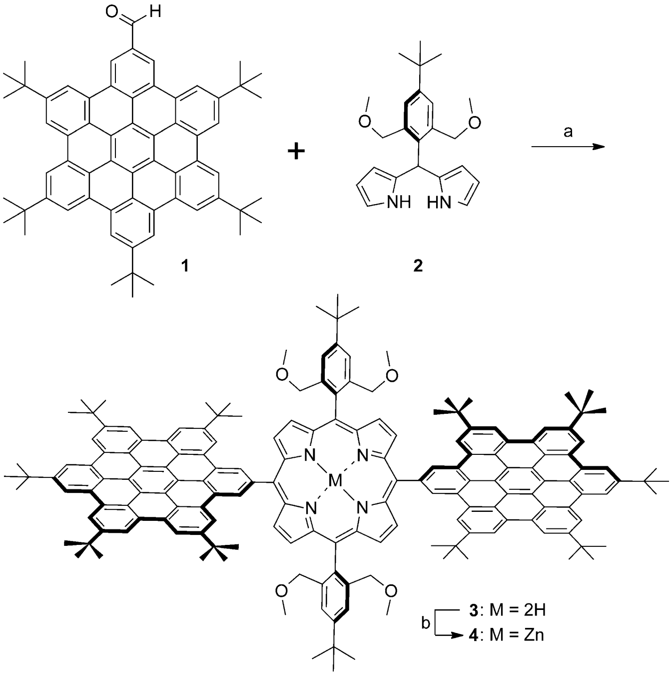

Scheme 1. Syntheses of free-base conjugate **3** and its Zn^{II} derivative **4**. a) cat. $BF_3 \cdot OEt_2$, cat. EtOH, $CHCl_3$, RT, then DDQ (M = 2H) (10%); b) $Zn(OAc)_2 \cdot 2\,H_2O$, THF, reflux (M = Zn) (100%).

---

[*] D. Lungerich, M. Marcia, Dr. F. Hampel, Prof. Dr. N. Jux
Department Chemie und Pharmazie & Interdisciplinary Center for Molecular Materials (ICMM)
Friedrich-Alexander-Universität Erlangen-Nürnberg
Henkestrasse 42, 91054 Erlangen (Germany)
E-mail: norbert.jux@fau.de

J. F. Hitzenberger, Prof. Dr. T. Drewello
Department Chemie und Pharmazie
Friedrich-Alexander-Universität Erlangen-Nürnberg
Egerlandstrasse 3, 91058 Erlangen (Germany)
E-mail: thomas.drewello@fau.de

[**] We thank the DFG (SFB 953, Synthetic Carbon Allotropes) for financial support.

Supporting information for this article is available on the WWW under http://dx.doi.org/10.1002/anie.201407053.

moiety at $\delta = -2.11$ ppm. The sharp signals indicate that there is no aggregation in solution.

The X-ray diffraction analysis (Figure 1) of a single crystal of **3**, grown at room temperature from a mixture of CH_2Cl_2, *n*-heptane, and methanol, represents the first crystallographic characterization of a superbenzene–porphyrin derivative and establishes its structure beyond any doubt.[9] The molecule crystallizes in a triclinic lattice with the space group $P\bar{1}$ and the unit cell contains six *n*-heptane molecules. The two HBC moieties are rotated by about 62.2° with respect to the porphyrin plane; the two *ortho*-disubstituted phenyl substituents are tilted by about 87.7° and stand almost perpendicular to the porphyrin plane. Both HBCs and the porphyrin core experience distortion in the crystal packing and lose their planarity. Although the HBC units are packed in parallel, the average distance between two overlapping HBC moieties is 7.36 Å and therefore π–π interactions in the solid state can be ruled out. In the rather large cavities between the HBC planes, *n*-heptane is entrapped rather unusually due to hydrogen–π interactions at a distance of 2.9–3.0 Å and acts essentially as an insulator. This is in striking contrast to what we found in a preliminary crystal structure of the zinc complex **4**.[10]

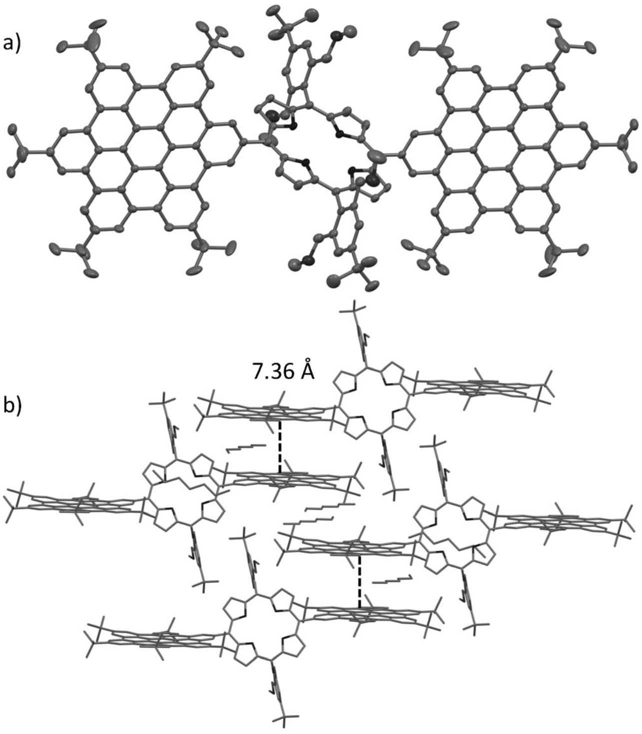

Figure 1. Crystal structure of free-base HBC–porphyrin conjugate **3** (hydrogen atoms are omitted for clarity). a) ORTEP model, b) crystal packing.

Interesting observations regarding the formation of aggregates of **3** have been made by mass spectrometry. MALDI-, LDI-, and ESI-MS were employed to characterize **3**. In MALDI, the observed molecular ion is abundant and accompanied by several cluster ions of the type $(\mathbf{3})_n^{+\bullet}$, as detected in linear ($n = 2$–6) and reflectron ($n = 2$) modes (Figure 2). Reflectron mode detection reveals that the clusters de-aggregate considerably as they pass through the mass spectrometer; only dimer $(\mathbf{3})_2^{+\bullet}$ in small amounts could be detected. This behavior is in line with the noncovalent nature of the bonding within the $(\mathbf{3})_n^{+\bullet}$ cluster ions. In experiments in which the decay behavior of size-selected cluster ions is studied (post source decay, PSD), the release of several moieties of **3** from the selected precursor ion is observed, which supports the assumption that the molecules of **3** retain their molecular integrity within the clusters. **3** itself showed the expected stability and formed abundantly intact molecular ions even under direct laser desorption/ionization (i.e. without matrix, LDI).

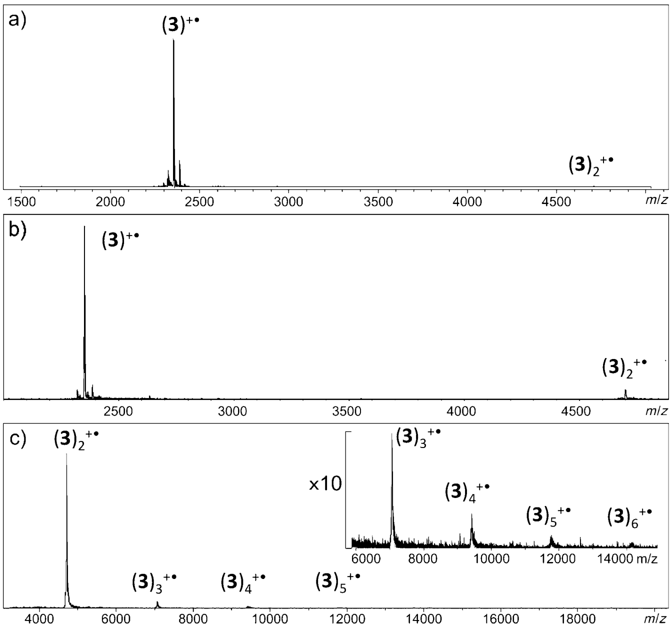

Figure 2. MALDI-TOF mass spectrum of **3** in the positive-ion mode; matrix: *trans*-2-[3-(4-*tert*-butylphenyl)-2-methyl-2-propenylidene]malononitrile (DCTB); radical cations are depicted as $(\mathbf{3})_n^{+\cdot}$. a) Reflectron mode detection, b) linear mode detection, c) as (b) with magnification of the larger clusters.

The propensity of **3** to form aggregates under the present conditions is quite remarkable compared to the clustering behavior of pentacene (**5**) and hexa-*tert*-butyl-hexa-*peri*-hexabenzocoronene (**6**). Clusters of compound **5** were observed previously in a dedicated high-pressure MALDI experiment, which promoted ion/molecule reactions and proved the existence of pentacene aggregates of the type $(\mathbf{5})_n^{+\bullet}$ with up to $n = 5$.[11] However, under the present conditions, neither **5** nor **6** show signs of higher aggregates, while **3** shows efficient cluster formation, underpinning the propensity of **3** to form aggregates under the applied conditions.

The ESI-MS shows the quasi-molecular ion peak of the protonated conjugate **3**, $\mathbf{3}H^+$, the isotope pattern of which confirms its identity and reveals the co-formation of doubly protonated dimer, $\mathbf{3}_2H_2^{2+}$. Besides protonation, oxidation of **3** occurs as an additional, competing ion-formation process.[12] The oxidation of **3** leads to the formation of the dication $\mathbf{3}^{2+}$, the trication $\mathbf{3}^{3+}$, and the trication of the dimer of **3**, $(\mathbf{3})_2^{3+\bullet}$.

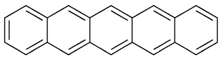

5

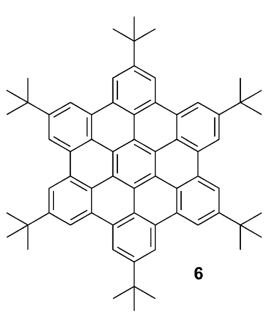

6

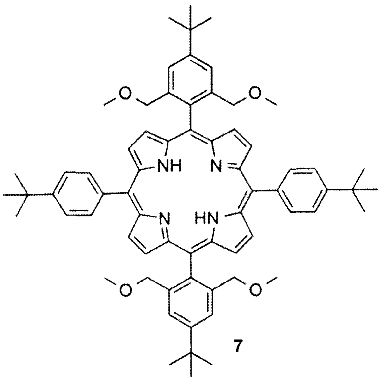

7

Small amounts of the dication $(\mathbf{3})_2^{2+}$ are also detected (Figure 3). The formation of a triply ionized dimer is most remarkable and particularly rare. It requires that the strength of supramolecular bonds between the two HBC–porphyrin conjugates **3** exceeds the Coulombic repulsion of the charges. The charges are distributed as in $\mathbf{3}^{2+}$–$\mathbf{3}^{+}$, since the dimer dissociates in collision-induced dissociations into the monomeric di- and radical cations. A possible charge distribution may involve the large HBC moieties, reducing Coulombic repulsion by separating the charges from each other as much as possible.

We assume that the dimer is formed in the electrospray process by the aggregation of two neutral molecules or by the clustering of one neutral and one already charged species. This process may be followed by further oxidation leading to the observed trication. Formation of the dimer from two already ionized monomers would require overcoming the Coulombic repulsion. The high oxidation state of the dimer may be favored under the applied spray conditions, since monomeric **3** also appears in the 2+ and 3+ charge states, while the radical cation is entirely absent. The fact that aggregates of **3** are formed both in MALDI and ESI experiments is indicative of the effective noncovalent interaction within the cluster. In light of the structural features of **3**, π–π radical cation interactions seem a likely source of the attractive forces in the gas phase, whereas X-ray and NMR analysis suggest a different explanation in the solid state and in solution. Clearly, the solvent plays a decisive structural role which is reflected in the results obtained by the methods of characterization.

Electronic interactions between the two HBC moieties and the porphyrin core have been thoroughly investigated in solution utilizing absorption and emission spectroscopy. The spectra are shown in Figure 4 and the spectroscopic details can be found in Table 1. The spectral features of porphyrin **3** are quite remarkable and the characteristic peaks of both HBC and porphyrin building blocks are visible. The same is true for the metalated derivative **4**. The absorption features of the conjugates are also affected by the electronic intramolecular communication between the HBC periphery and the porphyrin core. A comparison of their spectra with those of reference compound **6** and reference porphyrin **7**[7] allows for a better understanding of the optical properties of the conjugates.

First of all, both the β- and the *p*-band of the HBC residue are slightly hypsochromically shifted (ca. 2 nm) for **3** and **4**, with respect to reference **6**. Bearing in mind that two HBC units are present in the conjugate, the extinction coefficient (ε) at the λ_{max} value of the HBC region is decreased for both **3** and **4** with respect to the reference. For **3** this decrease in ε_{max} amounts to approximately 34%, which is already quite substantial, and for **4** it is even larger (ca. 52%). Furthermore, both **3** and—to a lesser extent—**4** exhibit a splitting of the porphyrin Soret band (B-band): the two peaks lie at 426 and 438 nm for **3** while they are at 434 and 444 nm for **4**. Additionally, the B-band of **3** is bathochromically shifted (on average 12 nm) and considerably reduced in intensity (by ca. 50%) with respect to reference porphyrin **7**. A similar red-shift, of about 5 nm, is observed for the Q-bands as well. Finally, the presence or absence of the central metal atom has a profound effect on the position/intensity of both the B- and Q-bands of the porphy-

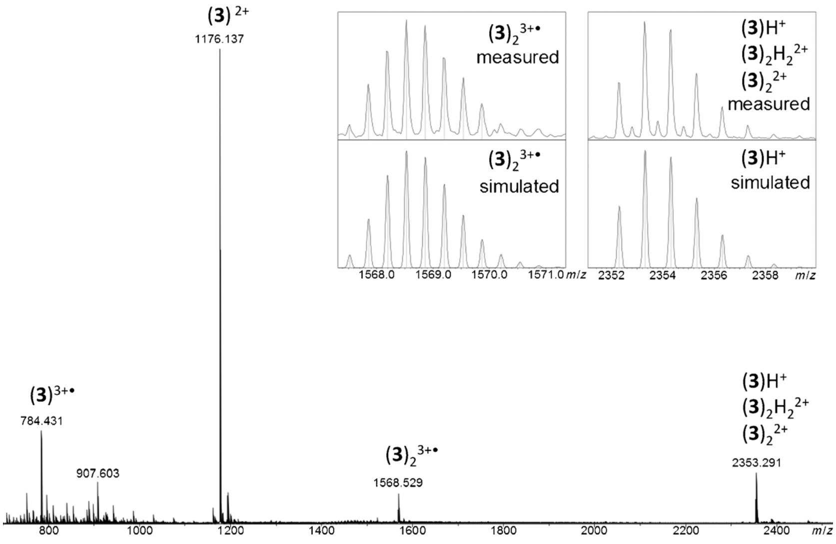

Figure 3. ESI-TOF mass spectrum of **3** in the positive-ion mode; the inserts show measured and simulated isotope patterns.

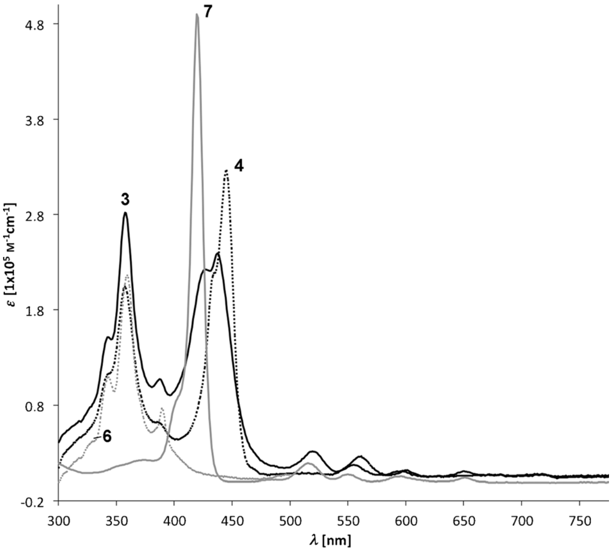

Figure 4. Absorption spectra of **3**, **4**, reference HBC **6**, and reference porphyrin **7**; $c = 2.5\cdot10^{-7}$ M in THF.

Table 1: Optical characterization in THF (see the Supporting Information).

	λ_{HBC} [nm] ($\log\varepsilon_{max}$) [$M^{-1}cm^{-1}$]	λ_{Porph} [nm] ($\log\varepsilon_{max}$) [$M^{-1}cm^{-1}$]	$\lambda_{Fluo,HBC}$ [nm] (Φ_{β})[a]	$\lambda_{Fluo,Porph}$ [nm] (Φ_{Soret})[a]
6	344, 360 (5.33), 389	–	474 (0.586), 483, 492, 517	–
7	–	419 (5.69), 515, 549, 592, 650	–	652 (0.033), 718
3	342, 358 (5.45), 388	426, 438 (5.39), 519, 555, 594, 650	469, 483 (0.073),[b] 493, 516	653 (0.059), 720
4	342, 357 (5.31), 386	434, 444 (5.52), 561, 600	469, 484 (0.111), 495	606 (0.076), 658

[a] With reference to fluorescein in NaOH 0.1 M ($\Phi = 0.925$).[14]
[b] Underestimated due to lamp interference.

rin unit. Comparing the spectra of **3** and **4**, it becomes evident that $\lambda_{max,Porph}$ is red-shifted upon metal insertion, from 438 nm to 444 nm. This is likely due to THF binding to the Zn ion. Additionally, the extinction coefficient of the higher peak of the B-band for the metalated derivative **4** (331 000 $M^{-1}cm^{-1}$) is drastically increased (ca. 26 %) with respect to the corresponding free-base porphyrin **3** (245 000 $M^{-1}cm^{-1}$). Upon metal insertion, position and intensity of the Q-bands are also affected with respect to free-base porphyrin. In our case, the absorption spectrum of **3** contains four Q-bands situated at 519, 555, 594, and 650 nm with decreasing intensity, while in the case of **4** only two bands are visible, located at 561 and 600 nm.

To highlight the profound electronic communication between the HBC and the porphyrin units, color contour plots of excitation versus emission for both conjugates **3** and **4** are presented in the Supporting Information (see Figures S3, S7, and S11). The superbenzene–porphyrin conjugate introduces a drastic quenching of the HBC emission in both **3** and **4** with respect to reference **6**. Upon excitation at λ_{max} of the β-band of HBC in the conjugate, however, strong fluorescence from the porphyrin's Q-bands can be detected. Upon excitation at $\lambda_{max,Porph}$ in the conjugate, no emission from the HBC moiety is present and only fluorescence from the porphyrin's Q-bands is observed. A possible explanation for the quenching of the HBC emission may be the occurrence of an electron/energy transfer from HBC towards the porphyrin core, which has been observed previously for structurally related porphyrin conjugates.[13] Interestingly, excitation at $\lambda_{max,HBC}$ in the conjugate results in a significantly higher intensity for the emission profile of **3** and **4** than excitation at $\lambda_{max,Porph}$. Additionally, excitation at $\lambda_{max,Porph}$ leads to a higher emission for the metalated derivative **4**. Further investigations, such as the determination of redox properties,[15] are necessary in order to shed more light on this phenomenon though.

In conclusion, a novel and versatile HBC-aldehyde building block (**1**) has been designed and used to construct the new porphyrin derivatives **3** and **4**. A single-crystal X-ray diffraction of HBC–porphyrin conjugate **3** gave insight into the structural packing of such carbon-rich porphyrin conjugates. MALDI measurements revealed the pronounced tendency of **3** to form clusters as big as $(\mathbf{3})_6^{+\bullet}$. Furthermore, ESI experiments showed that **3** undergoes a remarkable dimer formation to the species $(\mathbf{3})_2^{3+\bullet}$, whose attractive forces (presumably π–π or π–CH interactions) are strong enough to overcome Coulombic repulsion. Absorption and emission spectroscopy revealed a strong electron/energy transfer between the two chromophores, which results in unique absorption and emission features. The combination of these two unique subunits opens the door to further detailed optical characterization by, for example, ultrafast spectroscopy and spectro-electrochemistry. Moreover, such derivatives could pave the way for the construction and investigation of tailor-made carbon-rich supramolecular architectures, with feasible applications in the field of molecular electronics. Other HBC substitution patterns as well as other HBC–porphyrin conjugates are currently under investigation.

Received: July 9, 2014

Keywords: arenes · clusters · organic synthesis · porphyrinoids · structure elucidation

---

[1] V. V. Diev, C. W. Schlenker, K. Hanson, Q. Zhong, J. D. Zimmerman, S. R. Forrest, M. E. Thompson, *J. Org. Chem.* **2012**, *77*, 143–159.
[2] J. P. Lewtak, D. T. Gryko, *Chem. Commun.* **2012**, *48*, 10069–10086.
[3] a) S. Ito, P. T. Herwig, T. Böhme, J. P. Rabe, W. Rettig, K. Müllen, *J. Am. Chem. Soc.* **2000**, *122*, 7698–7706; b) J. Wu, M. D. Watson, N. Tchebotareva, Z. Wang, K. Müllen, *J. Org. Chem.* **2004**, *69*, 8194–8204.
[4] J. Wu, W. Pisula, K. Müllen, *Chem. Rev.* **2007**, *107*, 718–747.
[5] J. M. Englert, J. Malig, V. A. Zamolo, A. Hirsch, N. Jux, *Chem. Commun.* **2013**, *49*, 4827–4829.

[6] A. Hirsch, A. J. Kratzer, D. Lungerich, J. M. Englert, F. W. Heinemann, N. Jux, *Faraday Discuss.* **2014**, DOI: 10.1039/C4FD00069B.

[7] N. Jux, *Org. Lett.* **2000**, *2*, 2129 – 2132.

[8] J. S. Lindsey, I. C. Schreiman, H. C. Hsu, P. C. Kearney, A. M. Marguerettaz, *J. Org. Chem.* **1987**, *52*, 827 – 836.

[9] Refined formula $C_{214}H_{260}N_4O_4$, $M_r = 2952.26$, crystal dimensions $0.2878 \times 0.0858 \times 0.0451$ mm^3, triclinic, space group $P\bar{1}$, unit-cell dimensions $a = 16.7770(7)$, $b = 16.7834(7)$, $c = 20.4679(8)$ Å, $\alpha = 101.505(4)$, $\beta = 95.831(3)$, $\gamma = 119.864(4)°$, $V = 4758.7(3)$ Å^3, $Z = 1$, $\rho_{\mathrm{calcd}} = 1.030$ mg mm^{-3}, linear absorption coefficient $\mu = 0.448$ mm^{-1}, radiation/wavelength Cu$_{K\alpha}$/0.15418 nm, temperature of measurement 173.0(2) °C, $2\theta_{\max} = 6.26 – 117.86°$, no. of measured reflections 28484, no. of independent reflections 13628, $R_{\mathrm{int}} = 0.0494$, final R indexes [$I \geqq 2\sigma(I)$]: $R_1 = 0.0806$, $wR_2 = 0.2516$, final R indexes [all data]: $R_1 = 0.0957$, $wR_2 = 0.2728$, residual electron density 0.98/−0.31 e Å^{-3}. CCDC 945391 contains the supplementary crystallographic data for this paper. These data can be obtained free of charge from The Cambridge Crystallographic Data Centre via www.ccdc.cam.ac.uk/data request/cif.

[10] X-ray structure analysis of a non-single crystal of **4**, grown from CH_2Cl_2, indicates a π–π interaction distance of the HBC planes of 3.5–3.9 Å; see Figures S12 and S13 in the Supporting Information.

[11] S. V. Shcherbyna, D. K. Bohme, *J. Am. Soc. Mass Spectrom.* **2006**, *17*, 222 – 229.

[12] a) T. Drewello, H. Frauendorf, R. Herzschuh, A. A. Goryunkov, S. H. Strauss, O. V. Boltalina, *Chem. Phys. Lett.* **2005**, *405*, 93 – 96; b) M. P. Barrow, X. Feng, J. I. Wallace, O. V. Boltalina, R. Taylor, P. J. Derrick, T. Drewello, *Chem. Phys. Lett.* **2000**, *330*, 267 – 274.

[13] C. Aurisicchio, R. Marega, V. Corvaglia, J. Mohanraj, R. Delamare, D. A. Vlad, C. Kusko, C. A. Dutu, A. Minoia, G. Deshayes, O. Coulembier, S. Melinte, P. Dubois, R. Lazzaroni, N. Armaroli, D. Bonifazi, *Adv. Funct. Mater.* **2012**, *22*, 3209 – 3222.

[14] D. Magde, R. Wong, P. G. Seybold, *Photochem. Photobiol.* **2002**, *75*, 327 – 334.

[15] For preliminary results, see Figures S19 and S20 in the Supporting Information.